Photometric Characteristics of the Recurrent Nova T Coronae Borealis

2025 Graduation Thesis
Researcher: [1] One Choi, Instructor: [1] Sunmie Park
Korea Science Academy of KAIST [1]
DECEMBER 15, 2025

Abstract

In this study, we analyzed the brightness variations of T Coronae Borealis, a symbiotic recurrent nova system consisting of a white dwarf and a red giant, and developed a DSLR-based photometric pipeline. By analyzing over 150 years of observational data from the AAVSO database and reviewing previous studies, we confirmed that T CrB exhibits variability on two distinct timescales. Short-period flickering on timescales ranging from seconds to tens of minutes originates from turbulence in the boundary layer of the white dwarf, while long-period variation of 113.78 days is attributed to the ellipsoidal effect of the red giant. In addition, we developed a Python-based program that automates the entire process—from converting CR3 RAW files captured by a Canon EOS R6 to FITS format, through image correction, photometry, and analysis—and made it publicly available on GitHub. Between April and July 2025, we obtained 918 images of T CrB; however, we were unable to identify subtle variations due to very low signal-to-noise ratios. Nevertheless, we verified that the program functions properly through comparison star photometry, and the developed methodology is immediately applicable to T CrB nova eruption observations. This study validated a DSLR-based photometric methodology, characterized the variability properties of T CrB through analysis of AAVSO data, and established a technical foundation for future nova eruption observations.

Keywords: Nova, T Coronae Borealis, Flickering, Boundary layer of a white dwarf, Photometry

1 Introduction

T Coronae Borealis (hereafter T CrB) is a symbiotic recurrent nova consisting of a white dwarf and a red giant, located approximately 3,000 light-years from Earth. In this binary system, the white dwarf has a mass of approximately $1.37M_{\odot}$ (solar masses), and the red giant possesses a massive atmosphere that transfers material to the central star. T CrB has historically produced bright eruptions (nova eruptions) in 1866 and 1946, and is predicted to erupt with a period of approximately 80 years. The recent brightness changes have drawn attention to the possibility of a re-eruption in 2026.

Particularly, the flickering phenomenon occurring on short timescales is a brightness variation caused by irregular material inflow and emission, providing important clues for studying the internal physical processes of systems like T CrB. Flickering is believed to be related to the boundary layer between the white dwarf surface and the accretion disk, or to turbulence within the disk, playing a key role in understanding the dynamics of accretion processes. Additionally, T CrB shows long-period variability corresponding to half of its orbital period, which is explained by the ellipsoidal effect due to tidal distortion of the red giant.

This study aimed to achieve three main goals. First, we developed a celestial photometry pipeline using a DSLR camera, automating the entire process from converting Canon CR3 RAW format to FITS format, through image correction, photometry, and analysis. Second, we analyzed long-term observational data from the AAVSO (American Association of Variable Star Observers) database to characterize the physical properties of T CrB's flickering and long-period variations. Third, we performed photometric observations to validate the developed pipeline and quantitatively assess observational limitations. Through this, we aimed to elucidate the physical connections between mass transfer and the boundary layer around the white dwarf, and establish a technical foundation for observing the impending nova eruption.

2 Theoretical Background

2.1 T Coronae Borealis (T CrB)

T CrB is a binary system located in the direction of the constellation Corona Borealis, also known by the nickname "Blaze Star." The two members of this system are extreme binaries that strongly interact with each other.

One of the two stars is an evolved red giant of spectral type M4.5 III, which is large and highly luminous, contributing significantly to the visible spectrum and luminosity of T CrB in its quiescent state. Particularly, the light curve in the long-wavelength region is dominated by variability according to orbital phase caused by the giant's pulsation and ellipsoidal shape. In reality, regular variations with an amplitude of approximately 0.6 magnitudes are observed due to the ellipsoidal effect of the giant, caused by distortion from gravitational interaction with the white dwarf companion. Additionally, the giant releases material through a strong stellar wind, which is supplied to the white dwarf.

The white dwarf in T CrB has a very large mass. In the Hα spectroscopic study by Stanishev et al. (2004)[1], the white dwarf mass was estimated to be $1.37 \pm 0.13 M_{\odot}$, which meets the conditions for the system to become a recurrent nova. Gas from the red giant accumulates in the gravitational well of the white dwarf, forming an accretion disk. Balmer line emission arising from this disk is observed. Indeed, the spectrum of T CrB shows strong H I Balmer series emission lines overlaid on the red giant's spectrum, originating from the disk orbiting the white dwarf and the surrounding nebula. Also, high-excitation He II 4686Å emission lines are occasionally detected, indicating the existence of a high-temperature region near the white dwarf surface, such as the boundary layer of the white dwarf.

The white dwarf and red giant orbit each other with an orbital period of approximately 227.6 days. The orbit is nearly circular, and the orbital inclination is estimated to be about 67°. The red giant fills its Roche lobe, supplying mass to the white dwarf through either Roche lobe overflow or stellar wind accretion. When mass accumulates on the white dwarf over an extended period, it triggers thermonuclear runaway, causing a nova eruption. T CrB has been classified as a recurrent nova after being observed to produce nova eruptions with a period of approximately 80 years since the late 19th century. This star produced nova eruptions in 1866 and 1946, with maximum brightness rising to approximately 2nd magnitude, then gradually fading and maintaining approximately 10th magnitude during decades-long quiescent periods. Astronomers predicted that this binary system would undergo a nova eruption between late 2024 and 2025 after exceeding the mass limit; however, as of 2025, no eruption has occurred. Recent studies predict that the nova eruption will proceed in early 2026.

One important characteristic of this star as a recurrent nova is that it shows intermittent active phases during the quiescent period between major eruptions. There was a slight brightness increase in the late 1930s, which is considered a precursor to the 1946 nova eruption. Recently, a super-active state starting in 2014 was reported[2], with brightness continuing to rise until mid-2016. During this period, T CrB showed unusual activity not only in visible light but also in X-ray and radio observations[3]. From 2018 onwards, the brightness gradually decreased, returning to quiescent-level brightness by around 2023, drawing the attention of many astronomers. Previous studies reported that T CrB's active phases are statistically similar to outburst phenomena of SU UMa-type dwarf novae[4]. According to this interpretation, T CrB's mass-falling disk may have released material accumulated over decades all at once, then lost material from the disk before the next nova eruption.

2.2 Flickering

Flickering before nova eruption is a commonly observed phenomenon in accreting systems, characterized by irregular brightness variations on very short timescales from seconds to minutes. The amplitude is typically about 0.1–0.5 magnitudes, and several mechanisms have been proposed for its exact origin. Various studies have suggested unstable material flow in the boundary layer, turbulence within the disk, and ejections as causes of flickering, and recent observational results suggest that variations in mass flow transmitted to the white dwarf are the main cause of the flickering phenomenon[5].

Theories about flickering generation mechanisms can be broadly summarized into three categories.

First is variation in mass inflow rate. If the inflow rate of gas supplied from the companion to the white dwarf fluctuates at short time intervals, the radiation emitted from the accretion disk or boundary layer can change rapidly, causing flickering. For instance, pulsation of the red giant, temporary amplification of stellar wind, or inflow of fragmented material clumps can cause instantaneous increases and decreases in light output. Indeed, long-term observations in the ultraviolet band explain that such flickering is due to variable material inflow rather than orbital period effects.

Second, turbulence and viscosity instabilities within the disk have been proposed as causes. The mass-falling disk transports material and angular momentum through viscosity according to classical models. This viscosity is explained by turbulence in modern theory, and turbulent flow is inherently random, showing different brightness outputs at different times. Observationally, the spectrum of flickering signals shows a strong form at low frequencies, suggesting turbulent processes[6].

Finally, there is an explanation as a phenomenon due to material inflow in the boundary layer. In the innermost region of the accretion disk, disk material rotating rapidly decelerates just before contacting the white dwarf surface, forming a boundary layer. This boundary layer is a region where much of the accretion energy is radiated as high-energy electromagnetic waves such as X-rays or ultraviolet rays, with increased turbulence and shocks. Observationally, flickering signals appear in high-energy spectra in several systems including T CrB, suggesting that flickering originates at the boundary between the white dwarf and the disk[7]. Additionally, magnetic reconnection phenomena in strong magnetic fields within the boundary layer and inside the disk can also trigger flares, contributing to brightness variations.

Furthermore, a clear positive correlation exists between the amplitude of observed flickering and average brightness; the brighter the average brightness, the proportionally larger the flickering amplitude[5]. This means that the energy release process in the boundary layer near the white dwarf surface is relatively linear. Indeed, Ilkiewicz et al. (2016) showed through optical and X-ray observations that the flickering amplitude in T CrB is directly proportional to the average flux[5], particularly confirming that flickering appears more prominently in high-energy wavelength bands.

T CrB's flickering is mainly clearly detected in the ultraviolet to blue-light bands. This is because, as wavelength increases, variations are very small compared to the bright radiation of the red giant. In the U-band, the contribution of the red giant is small, so the brightness of the white dwarf and disk dominates, resulting in prominent flickering. In actual observations, typical flickering patterns with T CrB's U-band magnitude fluctuating in a sawtooth pattern on hour-long timescales have been recorded several times. Analyzing the full spectrum of this variation yields a typical power spectrum tilted toward the low-frequency band, as mentioned earlier.

Zamanov et al. (2004) introduced several characteristic parameters to quantify T CrB's flickering[7]. For example, they defined average brightness and flickering amplitude in certain time intervals and investigated the correlation between them. They also measured rms variation and autocorrelation time to observe statistical characteristics of flickering. This study found that flickering amplitude showed a strong correlation with the average brightness of that period. That is, the brighter the system, the larger the instantaneous flickering magnitude. Linear fitting on a log-log scale showed almost proportional increase. Also, T CrB's flickering power spectrum and temporal characteristics did not depend on average brightness. In other words, whether T CrB was in a dim or bright period, the distribution of frequency components or the shape of the autocorrelation function did not change significantly. This indicates that even when the overall state of the disk changes, the microscopic process creating flickering maintains similar dynamical characteristics.

2.3 Fourier Transform

The Fourier transform is a mathematical tool that analyzes any signal or function over time as a combination of various frequency components. Therefore, even complex functions can be represented as appropriate sums of trigonometric functions. In astronomy, it is used to analyze periodic components within brightness variations of stars as functions of time.

Assuming an arbitrary time function has periodicity, it can be expressed by transforming into a Fourier series as follows:

$$f(t) = \sum_{n=1}^{\infty} \left[a_n \cos\left(\frac{2\pi n t}{T}\right) + b_n \sin\left(\frac{2\pi n t}{T}\right) \right] \quad (1)$$

Through this, any periodic function can be completely decomposed into a sum of trigonometric functions with different frequencies. The mathematical reason this representation is possible is due to the orthogonality of cosine and sine functions. Orthogonality can be explained through integral relationships. Through this, any periodic function can be completely decomposed into a sum of trigonometric functions with different frequencies, and this decomposition is known to be unique.

For general functions without a defined period, the Fourier transform is applied instead of the Fourier series. At this time, the idea of extension is to assume that a general function has an infinitely large period. After extension, for continuous frequency components ω, the following integral form relationship is obtained:

$$F(\omega) = \frac{1}{\sqrt{2\pi}} \int_{-\infty}^{\infty} f(t) e^{-i\omega t} dt \quad (2)$$

$$f(t) = \frac{1}{\sqrt{2\pi}} \int_{-\infty}^{\infty} F(\omega) e^{i\omega t} d\omega \quad (3)$$

Here, $F(\omega)$ is the spectrum expressing the amplitude and phase of components at specific frequencies as complex numbers, and if the original function is known, a function for frequency components can be obtained. There is also an inverse Fourier transform that extracts the original function if the function for frequency components is known.

The Fourier transform defined above fundamentally deals with continuous functions. However, computers cannot process continuous data and handle discrete data sampled at regular time intervals. A modified Fourier transform for processing such discrete data is called the Discrete Fourier Transform (DFT). DFT calculates frequency components for a finite number of data points, but the computational complexity is proportional to the square of the number of data points

(N^2), so computation speed becomes very slow as data increases. The algorithm that dramatically reduced this long computation time is the Fast Fourier Transform (FFT). FFT greatly reduced computational complexity by eliminating redundant operations included in the DFT calculation process.

3 Research Methods and Procedures

3.1 T CrB Observation

Observations for this study were conducted at the Korea Science Academy observatory. As observation equipment, we used a 6-inch refracting telescope, the Takahashi TOA-150b model, and a Canon EOS R6 digital camera. The same camera and telescope combination was used in all observation sessions to maintain data consistency. Observations began after 9 PM following sunset to secure sufficient darkness by minimizing interference from sunlight.

Observations were conducted a total of 4 times on April 30, May 25, June 18, and July 21, 2025. Due to weather conditions, observation intervals were not fixed at exactly one month but were adjusted somewhat flexibly. On each observation date, observations started after 9 PM in the evening to measure the brightness of the target variable star T CrB, securing planned data.

The observation procedure was as follows. First, using TheSkyX astronomical software, we located T CrB's position and precisely aimed the telescope at the target object. Subsequently, through equatorial mount drive and TheSkyX's Earth rotation compensation function, the target object was maintained at the field center as much as possible during observation. Imaging was conducted in continuous observation form. Each frame's exposure time was set to 13 or 15 seconds, obtaining images at 30-second intervals. With these settings, multiple frames were continuously captured to observe brightness changes over time.

Appropriate exposure and ISO values were adjusted according to the ambient environment brightness or target object's instantaneous brightness on each observation date. Using Maxim DL software, we checked RGB channel values in three-dimensional graphs of real-time captured images to determine exposure time and ISO so that pixel saturation did not occur. Specifically, all images were set so RGB values did not exceed approximately 200, keeping starlight unsaturated and in the linear region. To meet these criteria, slightly different exposure times and ISO values were applied for each observation session.

After all main imaging (Light Frames) for the target object was completed, calibration images were captured. That is, dark frames (Dark), bias frames (Bias), and flat frames (Flat) were additionally obtained with the same camera and telescope settings. Dark frames were captured with the camera covered at the same exposure time and ISO as astronomical images to remove thermal noise generated as the CCD/CMOS sensor operates. Bias frames were captured with the camera covered at the shortest exposure time to calibrate the sensor's electronic offset and read noise. Flat frames were captured under uniform illumination to correct nonuniformities such as different sensitivities per sensor pixel and vignetting. These images were used in the data preprocessing stage for calibration.

Post-processing of collected observational data was performed through the aperture photometry method. Three comparison stars (HD 143352, HD 143256, HD 143161) with no brightness changes and known magnitudes were selected around the observed target star T CrB and imaged together. T CrB's relative brightness was calculated through differential photometry. Using the aperture photometry technique, brightness data for T CrB and comparison stars were extracted from each image, and T CrB's magnitude was calculated using comparison star magnitudes.

3.2 Data Analysis Plan

Data obtained through observation will be used to find brightness variation characteristics of T CrB through systematic analysis procedures. First, acquired CR3 RAW files are converted to FITS, the astronomical standard format, and systematic errors are removed through calibration using Bias, Dark, and Flat frames. Aperture photometry is performed on T CrB and surrounding comparison stars in calibrated images to measure flux changes over time. As comparison stars, HD 143352, HD 143256, and HD 143161, which are located within T CrB's field of view and known not to vary, were selected.

Differential photometry technique is applied to remove atmospheric extinction and instrumental effects. The ratio of T CrB's flux divided by comparison stars' average flux is calculated and converted to apparent magnitude using Pogson's equation. Through this, the influence of common factors such as atmospheric conditions or telescope tracking errors can be minimized. Photometry is performed independently for each RGB channel to compare and analyze variability characteristics according to wavelength. In particular, we aimed to confirm whether flickering is more prominent in blue light, confirming that the hot boundary layer is the main source of variability.

After creating a light curve over time, Fast Fourier Transform (FFT) is applied to search for dominant periodic components. Finally, we confirmed that our own observation results contained high levels of noise. However, we were able to evaluate T CrB's activity state during the observation period and validate the reliability of the photometric pipeline by comparing with long-term light curves from the AAVSO database. Detailed methodology for data processing and analysis will be covered in the next section.

4 Data Processing Methodology

4.1 Data Processing Pipeline Overview

In this study, we developed a professional data processing pipeline to transform and process celestial observation data acquired with a DSLR camera into a form suitable for scientific analysis. Canon Raw 3 (CR3) format RAW data captured with a Canon EOS R6 camera is a proprietary format that cannot be directly analyzed, so we implemented integrated software that automates the entire process from conversion to the astronomical standard format Flexible Image Transport System (FITS) to final photometric analysis.

Figure 1: The main GUI of the Toolbox

The entire pipeline consists of the following main stages. The first stage is RAW image conversion, decoding Bayer pattern data from CR3 files to generate linear RGB images and saving them in FITS format. The second stage is frame calibration, statistically combining Bias, Dark, and Flat frames to create respective Master frames, then Light frame calibration, using generated Master frames to remove systematic errors from the sensor in all astronomical images. The third stage is photometric analysis, tracking positions of target stars and comparison stars in calibrated images and performing aperture photometry to measure flux over time. The final stage is time series analysis, converting photometric data to differential magnitudes and performing Fourier analysis and statistical analysis to search for periodic components and flickering characteristics.

For pipeline implementation, Python 3.12 was selected as the base language, integrating several libraries specialized for astronomical data processing [Table 1]. The Rawpy library is a LibRaw Python wrapper supporting over 500 digital camera RAW formats and handles Canon CR3 file decoding. Astropy is the core Python package for astronomical research, providing FITS file I/O, time system conversion, and astronomical statistical functions. Photutils includes star detection, aperture photometry, and centroiding algorithms, while NumPy and SciPy provide the foundation for array operations and signal processing. Matplotlib was used for visualization, and the user interface was implemented with Tkinter, Python's standard library. These library choices were based on the stability of the open-source ecosystem and verified usage history in the astronomical community.

An important design philosophy of this software is intuitive operation through a graphical user interface. To enable astronomical researchers to perform complex data processing tasks without specialized programming knowledge, we provided GUI for all major functions. Tkinter, Python's standard library, was selected as the GUI framework, which has the advantage of requiring no additional installation and operating identically on all major operating systems: Windows, macOS, and Linux. Additionally, since Tkinter is the most widely used GUI tool in the Python community, maintenance and extension are easy. The GUI implemented through Tkinter has similar usage to HTML, and the final implemented GUI also resembles a website, allowing users to use it intuitively.

Most modules are designed to follow a consistent GUI structure. On the left or top of the window is a control panel providing input/output path selection, parameter settings, and execution buttons. On the right or center is a visualization area displaying processing results in real-time. At the bottom are a progress bar and status label indicating current task progress. Additionally, a log output window is provided where each processing step is recorded with timestamps, and detailed messages are displayed when errors occur. This consistency allows users to use new modules intuitively without additional learning when first encountering them.

Table 1. Python libraries used in the data processing pipeline

No.	Library	Description
1	Rawpy	LibRaw Python wrapper, supports 500+ camera RAW formats, Canon CR3 decoding
2	Astropy	Core package for astronomical research, FITS file I/O, astronomical statistical functions
3	Photutils	Star detection (DAOStarFinder), aperture photometry, centroiding algorithms
4	NumPy	Array operations and numerical computation base library
5	SciPy	Signal processing and scientific computing library
6	Matplotlib	Data visualization and graph plotting
7	Tkinter	GUI implementation Python standard library

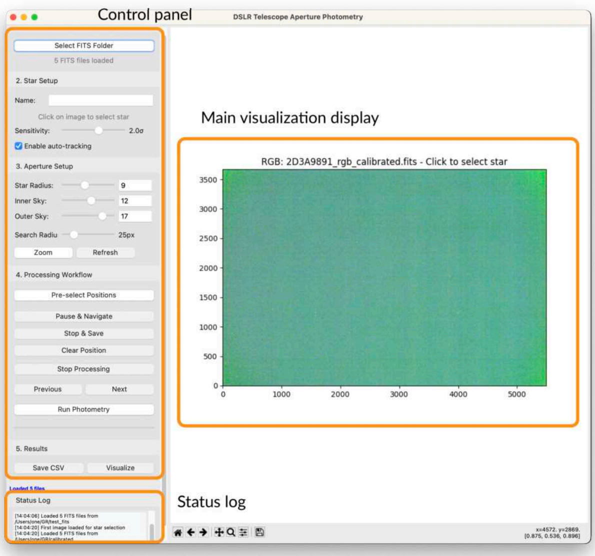

Figure 2: Standard GUI formation for each modules

Matplotlib graphs are directly embedded in the visualization area to enable real-time data verification. Matplotlib's GUI integration is implemented through the TkAgg backend, which converts Matplotlib figures into Tkinter widgets for insertion into windows. Backend setting must be performed before importing pyplot, specified with the matplotlib.use('TkAgg') command. Unlike other backends, TkAgg is known to work stably on all platforms, especially operating without problems in threaded environments. Embedded graphs provide basic tools such as Zoom, Pan, and Save, allowing users to examine results in detail.

4.2 CR3-FITS Conversion Module

A digital camera's image sensor cannot directly detect colors, so it arranges a color filter of red, green, or blue on each pixel to obtain color information. This arrangement method is called the Bayer pattern. Each photodiode on the sensor converts incident photons into electrons, and the number of electrons accumulated during exposure time is converted to digital values through an analog-to-digital converter. The Canon EOS R6 uses a 14-bit ADC, theoretically capable of representing values from 0 to 16383.

CR3 file decoding is performed through the LibRaw library. LibRaw is a C++ library extending dcraw's functionality, supporting over 500 RAW formats from major camera manufacturers including Adobe, Canon, Nikon, and Sony. Opening a CR3 file through Rawpy provides access to raw data in Bayer pattern and simultaneously parses EXIF metadata to obtain information such as exposure time, ISO sensitivity, shooting date and time, and white balance settings. This metadata is essential for determining calibration coefficients in subsequent processing stages or tracking data origin.

The extracted linear RGB data is saved in FITS, the astronomical standard format. The FITS format is a standard established by NASA and the International Astronomical Union, designed for exchange and long-term preservation of astronomical observation data. A FITS file consists largely of a header part and a data part. The header consists of ASCII text, with 80-character card images arranged consecutively. Each card consists of a keyword, equals sign, value, and optionally a comment. The data part is stored in binary format and supports multidimensional arrays.

When saving RGB images as FITS, array dimension order must be adjusted. The RGB array returned from Rawpy is generally structured in height, width, channel order. However, the FITS standard follows the convention of placing the fastest-changing axis last. Therefore, the array is transposed to rearrange in channel, height, width order. This way, each color channel forms an independent 2D image plane, making tasks like selectively reading only specific channels efficient.

The conversion module's GUI is designed with emphasis on batch processing functionality so users can process multiple CR3 files at once. At the top of the window are path input fields and browse buttons for selecting input and output folders. The input folder is the directory containing CR3 files to convert, and the output folder is the directory where generated FITS files will be saved. Paths can be typed directly or selected through a file selection dialog by clicking the browse button. Output format is selected from a dropdown menu between RGB FITS or Grayscale FITS. The Grayscale option converts RGB channels into a single channel using the ITU-R BT.601 standard luminance formula, reducing file size by approximately 1/3.

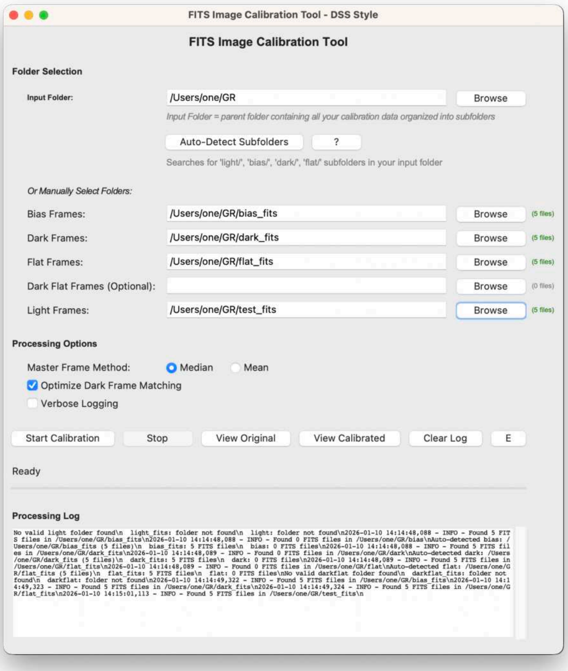

Figure 3: GUI for FITS image calibration module

Clicking the convert button automatically searches for all CR3 files in the input folder and performs conversion work for each file. Processing runs in a separate thread so the GUI does not freeze, and users can scroll the log or click the stop button during processing. The progress bar displays the percentage of files processed so far relative to total file count, and the status label shows the currently processing filename. The log window records each file's conversion start and completion with timestamps, and displays detailed error messages if errors occur. For example, errors such as unreadable damaged files, insufficient disk space, or no write permission to the output folder are clearly recorded.

Error handling is done on a per-file basis, so even if an error occurs in one file, the entire batch job is not interrupted. Files with errors are skipped and processing continues to the next file, leaving a failure mark in the log. When all files are processed, summary information is displayed, including total files, successful files, failed files, and total time taken. Users can save the log as a text file to later confirm which files failed and resolve problems. Typically, converting 100 CR3 files to RGB FITS takes approximately 5-7 minutes.

4.3 Calibration Module

Astronomical images contain not only pure signal from observation targets but also various systematic errors from the camera sensor and optical system. These errors are reproducible patterns that appear identically in all images, so they can be removed if properly measured and modeled. Standard CCD photometry techniques use three types of calibration frames to remove these errors. Bias frames measure the sensor's read noise and electronic offset, Dark frames measure dark current due to heat, and Flat frames measure vignetting of the optical system and sensitivity non-uniformity of the sensor. Additionally, Dark frame errors occurring in Flat can be removed to create cleaner Light frames. Darkflat is selectively included in calculations if provided; if left blank, it automatically excludes it from calculations and uses only the other three calibration frames. Multiple calibration frames of each type are captured and statistically combined to generate Master frames that minimize random noise.

Bias frames measure electronic errors occurring as the camera reads images. The sensor passes accumulated charge in each pixel through amplifiers and analog-to-digital converters to read it. During this process, thermal noise from amplifiers and quantization noise are added to the signal, called read noise. Read noise is random noise following a Gaussian distribution, with a mean of 0 but standard deviation having unique values for each sensor. Since Bias is a constant component independent of exposure time, it should be captured at the shortest possible exposure to minimize thermal noise contribution. For the Canon EOS R6 model, the minimum exposure time is 1/8000 second. The lens cap was completely closed to block external light sources, capturing 30 to 40 consecutive images. The reason for capturing multiple frames is to statistically remove random noise.

When generating Master Bias, median was used instead of arithmetic mean. The median is the value located in the middle when data is sorted by size, a robust statistic that can appropriately exclude extreme values. Since mean gives equal weight to all values, a single extreme value can significantly skew the overall mean. Conversely, median is not affected by extreme values, selecting only the value in the middle order. There are several reasons for preferring median in astronomical images. Hot pixels can have abnormally high values due to manufacturing defects or radiation damage, greatly increasing mean values but not affecting median. Sensor errors where some pixels read incorrect values temporarily can also be removed with median.

Dark frames measure the sensor's thermal noise. Silicon, a semiconductor material, spontaneously generates electron-hole pairs by thermal energy as long as it's not at absolute zero. Electrons generated this way cannot be distinguished from electrons generated by light, so they are added to the signal, called dark current. The magnitude of dark current depends on two main factors. First is exposure time; dark current is directly proportional to time. If the dark current rate per unit time is called the dark current rate, the total dark signal accumulated during exposure time t is the product of dark current rate and t. Therefore, Dark frames must be captured at the same exposure time as Light frames. If exposure times differ, they can be corrected by scaling ratios later, but capturing under identical conditions when possible is more accurate. Second is temperature; dark current increases exponentially with temperature. To minimize temperature effects, Dark frames were acquired immediately after Light frame capture. Ideally, alternating Light and Dark captures would track even instantaneous temperature changes, but in actual observations, all Lights were captured first followed by Darks for time efficiency. A waiting time of 30 seconds to 1 minute was allowed between each frame to prevent camera overheating from continuous shooting. Digital cameras heat up sensors and processors during continuous shooting, so appropriate cooling time is needed. When capturing Dark frames, exactly the same exposure time and ISO settings as Light frames were used. The lens cap was completely closed to block external light sources, excluding cases where some light leaks in and unintended signal is included in Dark frames.

Master Dark generation consists of two steps. First, Master Bias is subtracted pixel-by-pixel from each Dark frame. Since Dark frames also contain read noise and offset, removing them leaves only pure thermal noise. This step is expressed as follows:

$$\text{Dark}_{\text{corrected}} = \text{Dark} - \text{Master Bias} \tag{4}$$

Next, Master Dark is generated by median-combining Bias-removed Dark frames. The reason for using median is the same as for Master Bias, to remove effects of hot pixels and cosmic rays. Analyzing characteristics of generated Master Dark can reveal the sensor's thermal noise characteristics.

Flat frames correct non-uniform response characteristics of the optical system and sensor. In an ideal camera system, capturing a uniformly illuminated plane should result in all pixels having the same value. However, in reality, brightness varies spatially due to several factors. The most major cause is vignetting, where the image center is bright and edges are dark. Vignetting originates from the lens's optical characteristics and is classified into four types. Natural vignetting is the effect where effective aperture area decreases when light passing through the lens has an angle to the optical axis. Optical vignetting is the effect where lens barrel or lens elements block light at edges. Mechanical vignetting is the effect where filters or lens hoods partially obscure the field of view. Pixel vignetting is the effect where pixel microlenses cannot efficiently focus obliquely incident light.

Sensor sensitivity non-uniformity arises during manufacturing processes. Ideally, all pixels should have the same quantum efficiency, but in reality, factors such as impurity distribution in silicon crystals, doping concentration variations, and oxide layer thickness differences cause different quantum efficiencies per pixel. This pixel-to-pixel variation is typically at the 1-2

In the next step, corrected Flat frames are median-combined. Finally, normalization is performed. Normalization divides the entire frame by the mean or median value of each RGB channel so it becomes 1.0. The purpose is to ensure that the overall brightness scale of the image does not change after Flat correction. If not normalized and the Flat's average value is 30000, dividing the Light frame by this Flat would reduce all pixel values to 1/30000, making it abnormally dark. Making the mean 1.0 means dividing by approximately 1.0 at the center, so there's almost no change, and dark edges due to vignetting are divided by values less than 1.0, increasing brightness to make the whole uniform.

Light frame calibration is the process of removing systematic errors from all astronomical images using generated Master Bias, Master Dark, and Master Flat. The standard calibration formula is expressed as equation (4). Each pixel value of the calibrated image is calculated by subtracting Master Bias and scaled Master Dark from the original Light image, then dividing by normalized Master Flat.

$$\text{Calibrated} = \frac{I_{\text{light}} - I_{\text{bias}} - s_{\text{dark}} \times I_{\text{dark}}}{I_{\text{flat}}} \tag{5}$$

Here, s_{dark} is the Light frame's exposure time divided by the Dark frame's exposure time. In this study, Light and Dark exposure times were captured identically, so $s_{\text{dark}} = 1$.

Additionally, division by zero must be prevented. Some pixels in Flat frames may have very small values due to dust shadows or bad pixels. Dividing by values close to zero makes the result infinite or numerically unstable. To prevent this, a threshold of 0.1 was set, excluding pixels where Flat values are below the threshold from calibration. All of this process must calibrate each RGB channel independently. RGB images are 3D arrays, with the first axis representing channels.

4.4 Photometry Module

The photometry module is the core of this data processing pipeline, responsible for quantitatively measuring star brightness in calibrated images. Precise brightness measurement over time is essential for studying celestial object luminosity variations, so we implemented aperture photometry techniques. Aperture photometry is the most widely used photometric method in astronomy, summing all photons within a circular region defined around the star to obtain total flux. For accurate implementation, several techniques needed to be implemented in Python, including star position tracking, background sky removal, independent measurement per channel, and differential photometry.

The first step is finding star positions in images. Since hundreds of images need processing, automatic detection algorithms are essential. Star detection was performed using Photutils library's DAOStarFinder. DAOStarFinder was designed to perform accurate photometry even in crowded globular clusters or galaxy centers with many dense stars. Although the T CrB vicinity is not densely populated, DAOStarFinder's robust algorithms ensure stable detection in various situations.

The comparison stars selected in this study are HD 143352, HD 143256, and HD 143161. HD 143352 is a G-type main sequence star with V magnitude approximately 9.8, located about 15 arcminutes from T CrB. HD 143256 is a K-type main sequence star with V magnitude approximately 10.2, at about 12 arcminute distance. HD 143161 is a K-type main sequence star with V magnitude approximately 10.5, at about 18 arcminute distance. All are similar to T CrB's quiescent brightness of approximately 10th magnitude and located within the same field of view. Checking databases confirmed they were not classified as variable stars and had no interfering nearby stars.

The core of aperture photometry is defining a circular aperture containing the star and summing all pixel values within it. However, simply adding pixels within the aperture includes not only star signal but also background sky brightness. Background sky always has non-zero values due to airglow, galactic scattered light, and unresolved light sources from distant galaxies. Therefore, to obtain pure star flux, background must be separately measured and subtracted.

In aperture photometry, three concentric circles are used to measure star flux. The first is the aperture, a circular region containing the star; all pixel values within are summed to obtain total flux. The aperture radius is determined considering the star's point spread function; too small misses much starlight, while too large includes excessive background noise. Generally, 3-5 times the star's central brightness FWHM (full width at half maximum) is appropriate. The second and third circles form an annulus to measure background sky brightness. The annulus is a ring-shaped region outside the aperture; the median of pixels between inner radius and outer radius is estimated as background. The annulus size should be sufficiently distant from the aperture to avoid starlight influence, but not too far to reflect local background changes, typically set to 1.5-3 times the aperture radius range.

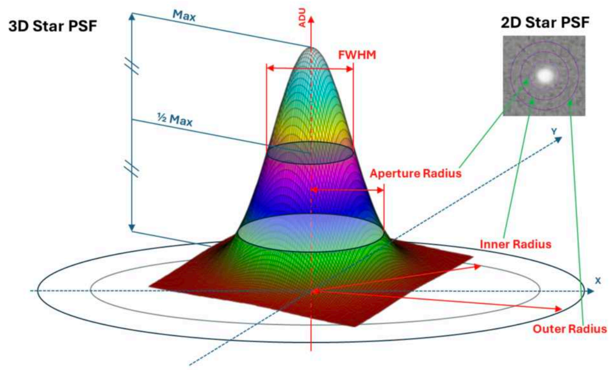

Figure 4: Aperture photometry [8]

RGB channel-by-channel photometry is performed as follows. Calibrated FITS files are 3D arrays in (3, H, W) format. The first axis represents channels, with 0 for Red, 1 for Green, and 2 for Blue. Photometry algorithms are applied independently for each channel. Using updated positions, aperture and annulus are defined and photometry performed. Background-subtracted flux is calculated and stored in channel-specific arrays. This procedure is repeated for Red, Green, and Blue channels. Performing this procedure for all frames yields three time series data. Flux-red[t], Flux-green[t], and Flux-blue[t] are Red, Green, and Blue fluxes at time t respectively. These can be analyzed individually or ratios calculated to obtain color indices.

Absolute photometry measures a star's actual magnitude, requiring standard star observations and atmospheric extinction correction. However, in variable star research, relative brightness changes are more important than absolute brightness, so differential photometry is used. Differential photometry observes non-varying comparison stars together, expressing target star brightness as relative values to comparison stars. The key idea of this method is that since the target star and comparison stars are observed through the same atmosphere, effects such as atmospheric extinction, clouds, and transparency changes are identical. Taking ratios cancels out these common factors.

In astronomy, magnitudes are typically used instead of flux. Magnitude is proportional to the logarithm of brightness, and the magnitude difference between two stars is defined by equation (6) according to Pogson's formula:

$$\Delta m = m_1 - m_2 = -2.5 \times \log_{10}\left(\frac{F_1}{F_2}\right) \tag{6}$$

The photometry module's GUI is the most complex and feature-rich. The left side is a control panel with controls for input FITS file folder selection, aperture parameter settings, star position specification, tracking option settings, background estimation method selection, and RGB channel selection.

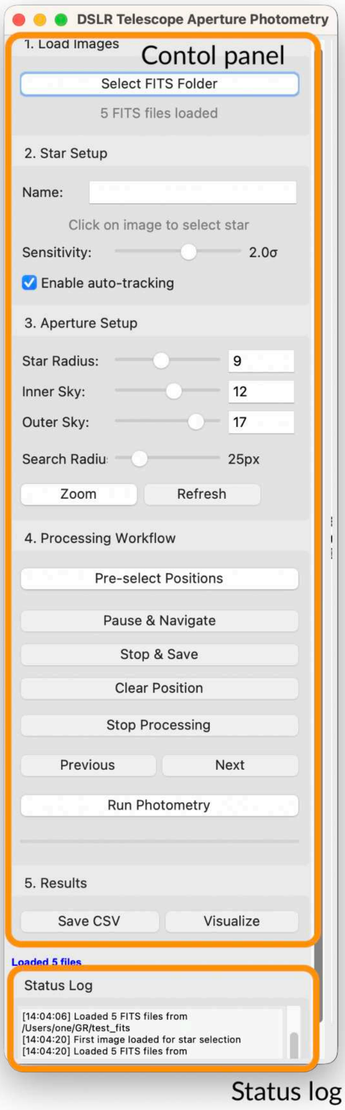

Figure 5: Aperture photometry GUI

Aperture parameters (aperture radius, annulus inner radius, annulus outer radius) can be adjusted via sliders or text input. Moving sliders updates apertures in real-time in the central display, providing visual feedback. Star position specification is performed by mouse clicking on the image display. When users click a star, that coordinate is saved and the aperture is displayed as an overlay.

The photometry execution process is as follows. When users select an input folder, all FITS files are automatically found and a list created. The first frame is loaded and displayed. Users view the image and click to select the target star and comparison stars. Aperture parameters are adjusted to set appropriate sizes.

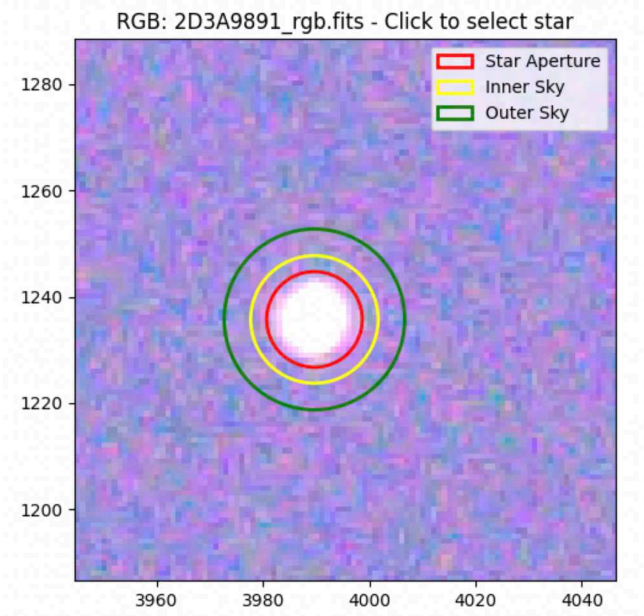

Figure 6: Example of aperture photometry for T CrB. Each radius is controlled individually

Once all settings are complete, star positions are first tracked. Processing is done for only one star at a time; if tracking multiple stars simultaneously, it's difficult to immediately detect when the tracking algorithm unintentionally switches to a nearby star, so it was designed to process only one star at a time. Extracting star positions first makes it advantageous to just redo photometry using different aperture sizes later. Multiple processes could have been combined into one, but considering research flow, stability, and intuitive program use, this was judged optimal. All processes display the current frame in real-time on the image display and mark selected positions. Users can pause or stop during processing. Pausing allows reviewing results so far, moving to previous frames if needed, manually adjusting positions, then resuming.

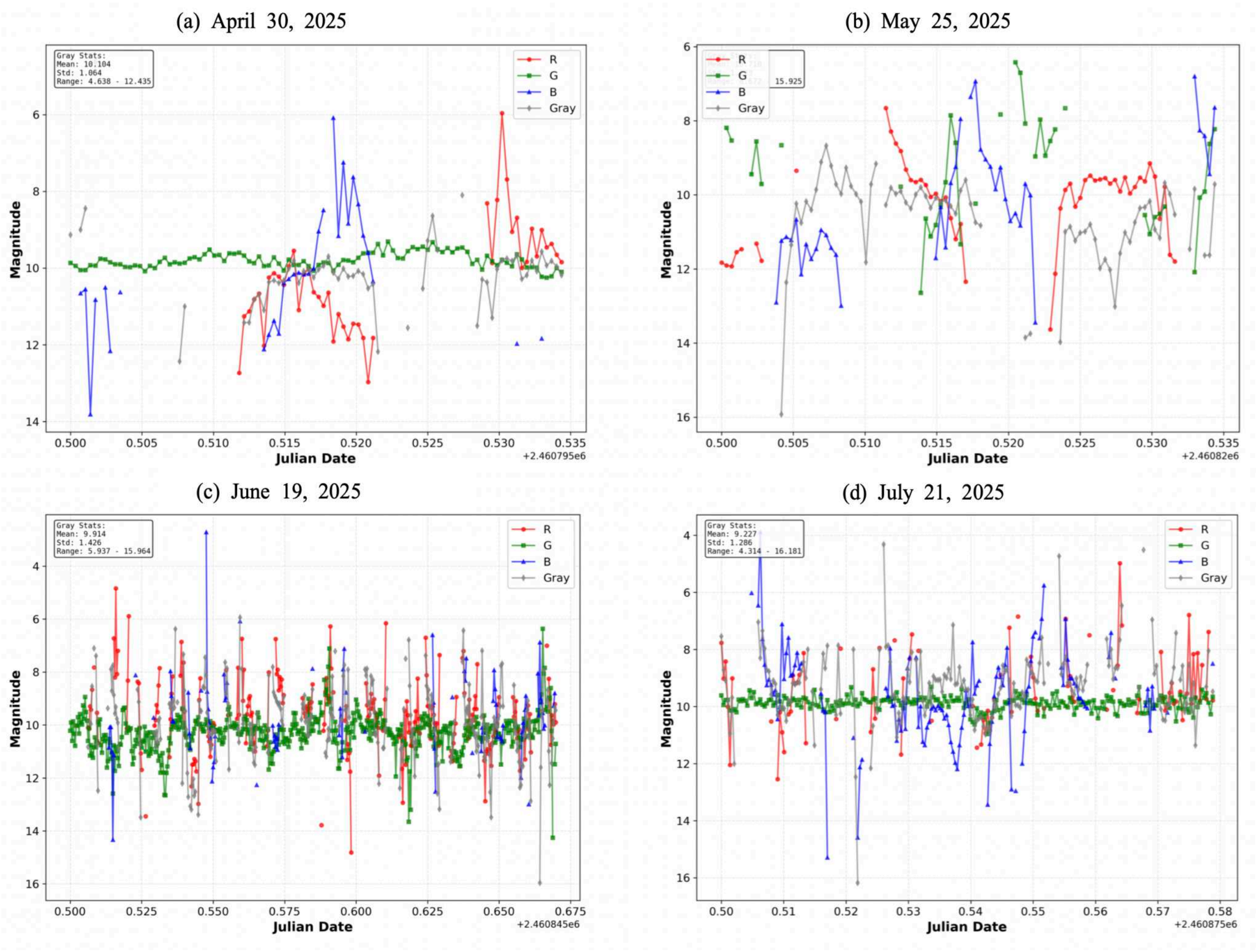

Figure 7: GUI for FITS image calibration module

5 Observation Results and Photometric Analysis

The most fundamental problem with photometry is that T CrB's signal is too weak compared to background noise. Directly checking intensity of FITS files after Maxim DL calibration showed background was approximately 1,800 to 2,200 ADU and T CrB's peak intensity was approximately 1,900 to 2,300 ADU (Analog-to-Digital Unit). The difference is only 100 to 300 ADU. That is, the star's pure signal is only about 5-15% of background, and in some frames the star and background were almost indistinguishable. This is because T CrB is inherently a dim object and due to the observation limit of the telescope used. Also, the Korea Science Academy observatory is not far from urban areas, so light pollution effects were likely significant.

Accordingly, negative fluxes frequently occurred when removing background after aperture photometry. When background flux is greater than total flux, the logarithm term in Pogson's equation becomes negative and cannot be calculated. This doesn't mean the star actually has negative brightness, a physically impossible situation, but indicates measurement limits were exceeded. This problem is that larger apertures include more background pixels, increasing the probability of negative values. However, making apertures too small misses much starlight. In this study, three combinations of aperture parameters (aperture radius, annulus inner radius, annulus outer radius) were tested: (9, 12, 17 pixels), (10, 15, 23 pixels), and (12, 17, 25 pixels), with (10, 15, 23 pixels) most appropriate but still experiencing negative problems. Although median is used in sky annulus to estimate background, if background itself has large local variations, it can be over- or underestimated. The exposure time of 13-15 seconds was set to prevent sensor saturation, but this simultaneously prevented sufficient signal accumulation. Using longer exposures increases star signal but also increases background noise with sensor saturation risk.

Figures [Fig. 7(a)]-[Fig. 7(d)] show T CrB photometry results collected over April 30, May 25, June 19, and

July 21, 2025. Differential photometry with comparison stars was performed using the self-developed magnitude analyzer program, displaying magnitude changes for each R, G, B filter along with grayscale magnitude. Grayscale magnitude was calculated applying weights of R:G:B = 1.852:1:1.613 based on Canon EOS R6's color response characteristics. Data distribution and quality differ for each observation date; April 30 and May 25 observations secured relatively few data points but showed clear variability patterns in R and B filters. June 19 observation secured the most data but showed large data scatter, and July 21 observation showed R and B filter variability at medium data density. Statistics (mean, median, range) for grayscale are provided in the upper left of each graph to quantitatively confirm average brightness level and variability range for each observation session.

Figure 8: Fourier transformation analysis of light curve of T CrB obtained on May 25, 2025

For example, [Fig. 8] is a periodogram created using Fourier transform based on May 25, 2025 observation data. The program presents the most dominant periodic component and its signal strength to quantitatively evaluate periodicity confidence. However, since this data has much noise and missing values were processed by linear interpolation, analysis result accuracy was expected to be limited.

Referring to the Periodogram in [Fig. 8], even in normally measured data, large variations of 1 to 2 magnitudes or more were observed. This is a combined result of T CrB's actual variability and photometric errors. According to literature, T CrB shows flickering of 0.1-0.5 magnitudes on minute to tens-of-minutes timescales. However, variations observed in this study are much larger. Due to low signal-to-noise ratio (S/N), photometric uncertainty exceeded 0.5 magnitudes, overwhelming actual variability signals. To verify whether this problem was due to software or methodology, the same photometry was performed on comparison stars. If there were bugs in software or algorithms were incorrect, comparison stars would also show random results. Analysis results showed all three comparison stars exhibited similar patterns of variation to T CrB [Fig. 9]. Comparison stars HD 143352, HD 143256, and HD 143161 all brightened or dimmed at similar times to T CrB in light curves. Since comparison stars are not physically variable stars, all observed variations are due to photometric errors or atmospheric condition changes.

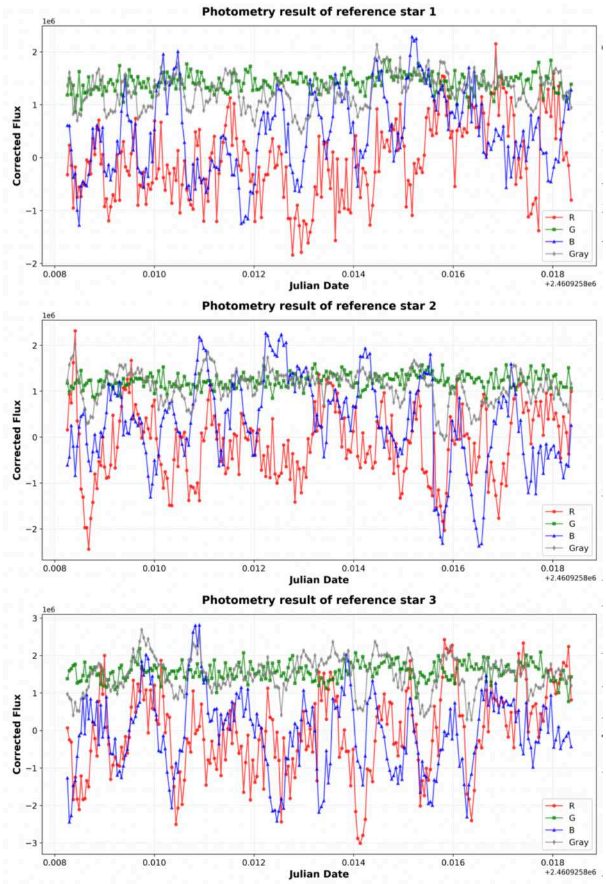

Figure 9: Consistent tendency of photometry graph in three reference stars

The important point is that comparison stars experiencing the same problems as T CrB means the photometry software itself is operating normally. If there were software bugs, comparison star results would be random or show different patterns. However, all stars show consistent trends, so the problem lies in observation conditions and target object brightness. This allows us to conclude that the developed software and methodology function properly.

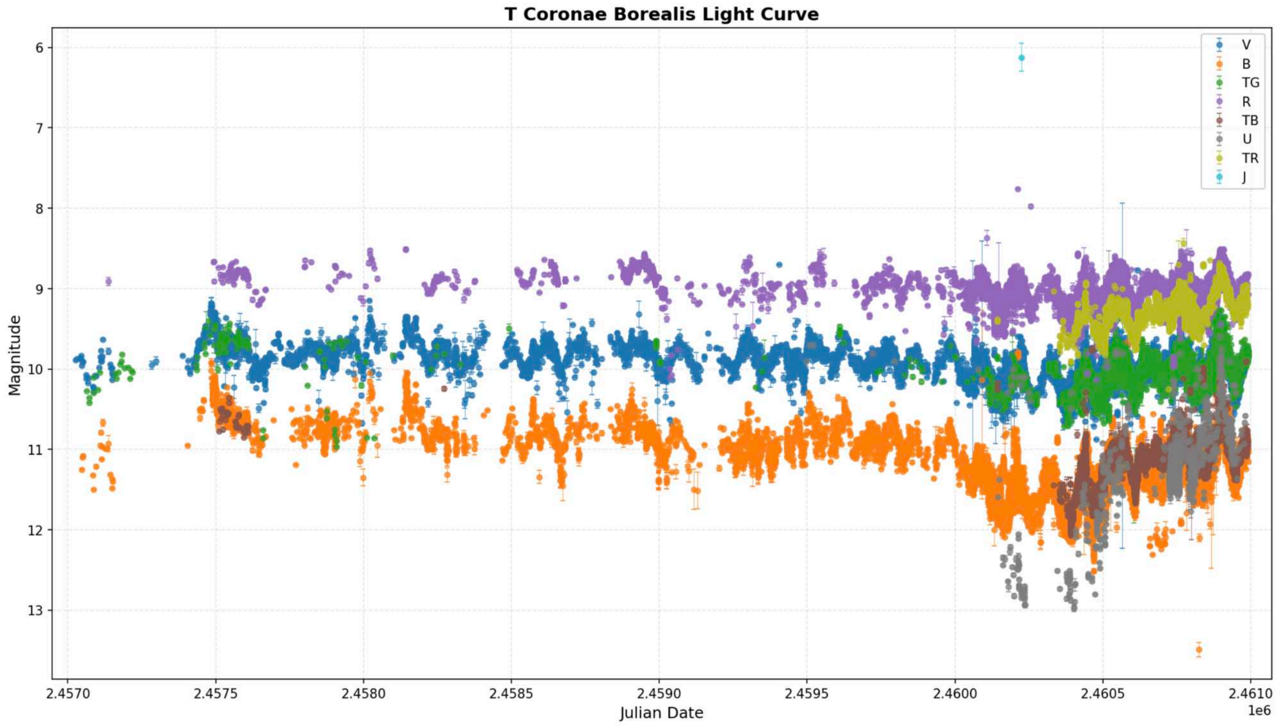

Figure 10: T CrB light curve from January 1, 2015 to December 1, 2025 (data from AAVSO)

6 Photometric Analysis and Brightness Variation Characteristics Study

6.1 Using AAVSO Database

After processing self-observed T CrB data using the developed photometry pipeline, noise levels were very high due to the star's low brightness (average $V \approx 10$ mag). Signal-to-noise ratio in images acquired with 13-second exposure was approximately 5-8, insufficient to reliably detect subtle variations below 0.1 magnitude. Particularly, studying flickering on short timescales requires high temporal resolution; increasing exposure time degrades temporal resolution, while decreasing exposure time further worsens signal-to-noise ratio.

To overcome these observational limitations and study T CrB's long-term variability characteristics, we utilized data from the American Association of Variable Star Observers (AAVSO). AAVSO, established in 1911, is an international association that has collected variable star observation data from amateur and professional observers worldwide, currently possessing over 54 million observation data points. All data is publicly available and freely usable for research purposes. The greatest advantage of AAVSO data is systematic observation records over long periods. For T CrB, over 150 years of observation data have been accumulated from after the 1866 nova eruption to present, allowing tracking of changes on timescales much longer than the orbital period (227.55 days). Data search was performed through AAVSO's web interface (https://www.aavso.org/data-download). In this study, we collected data from 2 years before and after the 1946 nova eruption (1944-1948) and from 2016 to present during the recent active period, using over 604,000 data points observed in Visual, V-band, and B-band filters for analysis. Downloaded data includes Julian Date, magnitude, uncertainty, filter, observer information, etc., and clearly outlying values and measurements with large uncertainty were excluded.

6.2 Two Timescales of T CrB Brightness Variation

[Fig. 10] is a multi-filter light curve of T Coronae Borealis from 2015 to present for approximately 10 years, referencing the AAVSO database. Data observed in various filters including V, B, TG, TB, Tr, I, J shows clear variability with a period of approximately 113 days, half the orbital period (approximately 227 days), interpreted as ellipsoidal variability according to the binary system's orbital motion. After transitioning to high state around 2015, it maintained a continuously brightened state, then significant dimming was observed in all filters from mid-2023. This is judged to be a pre-eruption dip similar to 1945-1946, and eruption before mid-2024 was expected. However, no eruption has occurred as of December 2025, and the system still maintains a dimmed state, increasing uncertainty about eruption timing.

Analyzing AAVSO data confirmed that T CrB shows brightness changes on two clearly distinguished timescales. The first is flickering occurring on short timescales from seconds to minutes, and the second is ellipsoidal variability appearing with a period of approximately 113.8 days, half the orbital period.

6.3 Physical Origin of Short-Period Flickering

Short-period flickering is a long-known phenomenon in variable star research, commonly observed especially in cataclysmic variables. Various researchers have performed high-speed photometry to quantify flickering characteristics. Zamanov et al. (2004) observed T CrB with UBV filters over 27 nights to investigate systematic characteristics of flickering[7]. Flickering amplitude is generally between 0.1-0.5 magnitudes, with occasionally large flares exceeding 1 magnitude observed. In this study's analysis using AAVSO data, due to time resolution limitations, flickering on second-scales could not be directly detected. Most AAVSO data was measured at intervals from minutes to hours.

Such short-timescale flickering is understood to originate from instabilities occurring in the boundary layer between the accretion disk and white dwarf surface. Material transferred from the red giant forms an accretion disk around the white dwarf through Lagrange points. Material in this disk moves inward in spiral orbits losing angular momentum through viscous friction. Due to originating from instability, no single period was discovered.

6.4 Physical Origin of Long-Period Ellipsoidal Variability

Variability appearing with a 113.78-day period, half the orbital period, has a completely different origin. This period can be seen to be exactly half of the red giant's orbital period of 227.55 days. This characteristic is mainly found in eclipsing binaries, but in T CrB's system this phenomenon occurs for a different reason. This is a geometrical effect occurring as the red giant is distorted into an ellipsoidal shape by the white dwarf's strong gravity. In the T CrB binary system, the red giant nearly fills its Roche lobe. Therefore, to express the red giant's shape more accurately, it's not a sphere but a long ellipsoid. The axis toward the white dwarf is longest, and the axis perpendicular to the orbital plane is shortest. As this ellipsoid revolves around the orbital plane, the projected area seen by observers changes. When the red giant is located on the side of the orbit, the ellipsoid's long axis is perpendicular to our line of sight, showing the widest area. These factors are presumed to cause long-period brightness changes.

6.5 Verification of Unusual Properties Reported in Previous Studies

T CrB is not a simple binary but a very complex object showing various behaviors, with various researchers reporting diverse unusual phenomena. In this study, we aimed to verify some of these characteristics using AAVSO data.

First is flickering's wavelength dependence. Zamanov et al. (2004) reported that flickering is strongest in U-band and weakens in B, V order[7]. This study also confirmed that B-band RMS variation (approximately 0.18 magnitudes) is larger than V-band (approximately 0.12 magnitudes), reconfirming that flickering is more prominent in blue light. This is because flickering originates in the hot boundary layer, and this region's radiation is dominant in blue and ultraviolet regions. The red giant's contribution is concentrated in red light, so in V-band and longer wavelengths, flickering signals are diluted by the red giant's stable luminosity.

Second is the very unusual phenomenon called pre-eruption dip. Schaefer (2023) discovered in historical observation records that T CrB suddenly dimmed for about 1 year before the 1946 nova eruption, then brightened with the eruption[8]. This dip showed approximately 1.5 magnitude decrease in B-band and approximately 0.8 magnitude in V-band. [Fig. 12] shows the visual magnitude light curve (AAVSO data) for ± 3 years around the 1946 eruption. The pre-eruption dip starting around 1945.0 (JD-2431500), approximately 1.1 years before eruption, shows dimming of approximately 2.5 magnitudes from 9.8 to 12.3 magnitude, darker than the red giant companion's intrinsic brightness, interpreted as due to dust formation in the line of sight. This dimming abruptly ended with the thermonuclear eruption on February 9, 1946, and the eruption increased to 3.0 magnitude then returned to normal state over several weeks. Remarkably, the same pattern was observed again starting from March 2023. Analyzing AAVSO data confirmed that T CrB maintained high brightness of the super-active phase until before March 2023, then began rapidly dimming from March.

The cause of pre-eruption dip is still debated. Either way, pre-eruption dip is interpreted as a precursor phenomenon signaling imminent nova eruption, and indeed in 1946, eruption occurred approximately 1 year after dip began. After the 2023 dip was discovered, many astronomers expected eruption between late 2024 and early 2025, but no eruption has occurred as of December 2025. This suggests either the time interval between dip and eruption is not 1 year, or other factors may influence eruption timing.

These various unusual phenomena show that T CrB is not a simple binary but a system with complexly intertwined physical processes including accretion disk, boundary layer, outward wind, intermittent jets, and dust generation. Multiple timescale variations including nova eruption period, super-active phase period, orbital period, and flickering overlap, making long-term and multi-wavelength observations essential for complete understanding. This study verified and quantified parts of this complex behavior utilizing AAVSO's rich database, and more detailed research is expected through additional observations in the future.

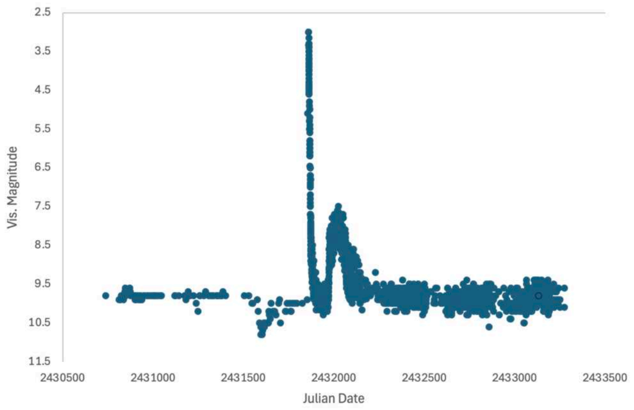

Figure 11: Light curve of T CrB in 1946, the year of eruption

7 Conclusion

In this study, we analyzed luminosity variations of the recurrent nova T Coronae Borealis and developed a DSLR-based photometry pipeline. Analyzing over 150 years of observation records from the AAVSO database and reviewing previous studies confirmed that T CrB exhibits variability on two timescales. Short-period flickering on timescales from seconds to tens of minutes originates from turbulence in the white dwarf boundary layer, showing a linear relationship between amplitude and average flux[5, 7]. Long-period variability of 113.78 days was confirmed as ellipsoidal effect due to tidal distortion of the red giant. Particularly, we discovered that the pre-eruption dip observed before the 1946 eruption has been reproduced since March 2023, capturing precursor phenomena of imminent nova eruption. Additionally, we developed Python software automating the entire process from converting CR3 RAW files captured with Canon EOS R6 to FITS, through calibration, photometry, and analysis, and made it publicly available on GitHub.

Through our own observations, we acquired 918 T CrB images through a total of 4 observations from April to July 2025, but T CrB's (brightness $V \approx 10$ mag) signal-to-noise ratio (S/N) was very low at 5-8, unable to detect subtle variations below 0.1 magnitude. However, we verified that the software operates normally through comparison star photometry and confirmed the 150mm telescope's observation limits. The software and methodology developed in this study can be applied to T CrB nova eruption observations. During nova eruption, T CrB is expected to brighten over 100 times to reach $V \approx 2$ magnitude, allowing acquisition of high-quality observation data even with small telescopes. Therefore, this study completed technical preparation for observing the historical astronomical phenomenon reproduced after 80 years.

Future research needs to strengthen observation capability using larger telescopes and cooled cameras, and expand software functions including PSF photometry and cosmic ray rejection. Additionally, through multi-wavelength collaborative observations using space telescopes like Swift or XMM-Newton and participation in international observation campaigns, T CrB's physical characteristics can be studied more deeply. This study established DSLR photometry methodology, confirmed T CrB's complex variability phenomena through AAVSO data analysis, and contributed to symbiotic recurrent nova research by establishing a technical foundation for observing imminent nova eruption.

References

[1] Stanishev, V., Zamanov, R., Tomov, N., & Marziani, P. (2004). The white dwarf mass in the recurrent nova T Coronae Borealis. *Astronomy & Astrophysics*, 415, 609–615.

[2] Luna, G. J. M., Sokoloski, J. L., Patterson, J., & Mukai, K. (2019). The super-active state of T Coronae Borealis. *The Astrophysical Journal*, 880(2), 94.

[3] Luna, G. J. M., Sokoloski, J. L., Mukai, K., & Sion, E. M. (2018). An extended X-ray outburst from the symbiotic recurrent nova T Coronae Borealis. *The Astrophysical Journal Letters*, 852(1), L1.

[4] Ilkiewicz, K., Mikołajewska, J., Monard, B., & Gromadzki, M. (2016). Discovery of a new superoutburst in T Coronae Borealis. *Astronomy & Astrophysics*, 585, A128.

[5] Ilkiewicz, K., Mikolajewska, J., Stoyanov, K., Manousakis, A., & Miszalski, B. (2016). Active phases and flickering of a symbiotic recurrent nova T CrB. *Monthly Notices of the Royal Astronomical Society*, 462(3), 2695–2704.

[6] Lyubarskii, Y. E. (1997). Flicker noise in accretion discs. *Monthly Notices of the Royal Astronomical Society*, 292(3), 679–685.

[7] Zamanov, R. K., Gomboc, A., Bode, M. F., Schmidtobreick, L., Bachev, R., Bellas-Velidis, I., Boumis, P., Dimitrov, D., Garrido, J. L., Ovcharov, E., Puschmann, K., & Stoyanov, K. A. (2004). Rapid optical flickering of T Coronae Borealis. *Monthly Notices of the Royal Astronomical Society*, 350(3), 1477–1486.

[8] Schaefer, B. E. (2023). Precursor and Decline Light Curves of T CrB from 1842 to 2021. *The Astrophysical Journal*, 950(2), 145.